

AD-A257 226

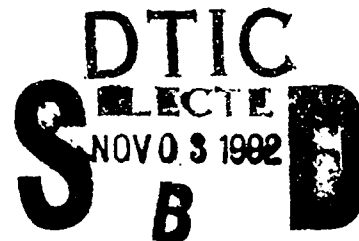


Rensselaer

Richard E. Lahey, Jr.
Edward E. Hart, Jr. Professor of Engineering

October 22, 1992

Dr. Edwin P. Rood
Scientific Officer Code: 1132F
Office of Naval Research
800 North Quincy Street
Arlington, VA 22217-5000



Dear Dr. Rood:

The purpose of this letter is to transmit the seventh quarterly report for ONR Grant N00014-91-J-1271, "An Experimental Study of Plunging Liquid Jet Induced Air Carryunder and Dispersion" (Lahey & Drew - CoPI).

This report period has been primarily concerned with the development of a two-fluid Computational Fluid Dynamics (CFD) model for a free two-phase jet. This model has been implemented into PHOENICS and evaluated on a RISC/6000 work station and the CRAY YMP-8 at Stennis Space Center.

We first present a state-of-the-art two-fluid model for air/water flows, which consists of the phasic three-dimensional conservation equations of mass and momentum. The associated closure conditions will also be discussed, along with some general constraints, followed by specific constitutive relations for low void fraction bubbly two-phase flows. Finally, the results of the numerical evaluation of a planar plunging liquid jet will be presented.

For isothermal, incompressible air/water flows the appropriate ensemble averaged conservation equations for a free two-phase jet are:

Mass Balance

$$\frac{\partial(\alpha_k \rho_k)}{\partial t} + \nabla \cdot (\alpha_k \rho_k \mathbf{v}_k) = 0 \quad (k = g \text{ or } l) \quad (1)$$

DISTRIBUTION STATEMENT A

Approved for public release
Distribution Unlimited

92-28669



Momentum Balance

$$\frac{(\alpha_k \rho_k \underline{y}_k)}{\partial t} + \nabla \cdot (\alpha_k \rho_k \underline{y}_k \underline{y}_k) = \nabla \cdot [\alpha_k (\underline{T}_k + \underline{T}_k^{Re})] + \alpha_k \rho_k \underline{g} + \underline{M}_{ki} \quad (k = g \text{ or } \ell) \quad (2)$$

Interfacial Jump Conditions

$$\underline{M}_{gi} = - \underline{M}_{\ell i} + \nabla \cdot [\alpha_g (\underline{\sigma}_s + (p_{gi} - p_{\ell i}) \underline{I})] \quad (3)$$

where,

$$\underline{T}_k = - p_k \underline{I} + \underline{\tau}_k \quad ; \quad p_{gi} - p_{\ell i} = 2\sigma/\bar{R}_b$$

and the surface stress tensor is

$$\underline{\sigma}_s \triangleq \rho_\ell [\hat{a}_s \underline{y}_r \underline{y}_r + \hat{b}_s (\underline{y}_r \cdot \underline{y}_r) \underline{I}]$$

which a sphere,

$$\hat{a}_s = - \frac{9}{20} \quad , \quad \hat{b}_s = \frac{3}{20}$$

In these conservation equations, α_k is the volume fraction corresponding to phase-k, ρ is density, \underline{y} is velocity, \underline{T} is the total stress tensor, \underline{g} is gravity and \underline{M}_{ki} is the interfacial force (per unit volume).

Because of the averaging process the system of equations have more unknowns than equations. In order to have a closed mathematical system one must constitute the interfacial momentum transfers and the Reynolds stresses.

One simple way of constituting the interfacial momentum transfers is by assuming that the only source of interfacial momentum interchange is drag. The algebraic drag law which is normally used is:

$$\underline{M}_i^D = \frac{3}{4} C_D \frac{\rho_\ell}{D_b} \alpha_v |\underline{y}_r| \underline{y}_r \quad (4)$$

* Note in the attached figures, $\alpha_g \equiv \epsilon$.

For	
Dist	<input checked="" type="checkbox"/>
Avail	<input type="checkbox"/>
Special	<input type="checkbox"/>
Availability Code	
Dist	
A-1	

ADA243815

where \bar{D}_b is the mean bubble diameter and C_D is the drag coefficient. A well known drag correlation due to Wallis is:

$$C_D = \frac{6.3}{\bar{R}_b^{0.385}} \quad ; \quad Re_b = \frac{\bar{D}_b |\underline{u}_r|}{\nu_\ell} \quad , \quad \underline{u}_r = \underline{u}_g - \underline{u}_\ell$$

The phasic momentum equations of the resultant two-fluid model are given by:

$$\begin{aligned} \frac{\partial}{\partial t} (\alpha_g \rho_g \underline{v}_g) + \nabla \cdot (\alpha_g \rho_g \underline{v}_g \underline{v}_g) = \nabla \cdot [\alpha_g \underline{\sigma}_s] + \nabla \cdot [\alpha_g (\underline{T}_g + \underline{T}_g^{Re})] \\ - \alpha_g \nabla p_\ell + \alpha_g \rho_g \underline{g} - \frac{C_D}{8} \rho_\ell A_i''' \underline{v}_r |\underline{v}_r| \end{aligned} \quad (5a)$$

$$\begin{aligned} \frac{\partial}{\partial t} (\alpha_\ell \rho_\ell \underline{v}_\ell) + \nabla \cdot (\alpha_\ell \rho_\ell \underline{v}_\ell \underline{v}_\ell) = \nabla \cdot [\alpha_\ell (\underline{T}_{\ell(BI)}^{Re} + \underline{T}_{\ell(SI)}^{Re})] \\ - \alpha_\ell \nabla p_\ell + \alpha_\ell \rho_\ell \underline{g} + \frac{C_D}{8} \rho_\ell A_i''' \underline{v}_r |\underline{v}_r| \end{aligned} \quad (5b)$$

where $\underline{T}_{(BI)}$ is the stress tensor corresponding to bubble-induced pseudo-turbulence and $\underline{T}_{(SI)}$ is the stress tensor corresponding to shear-induced turbulence. The later stress tensor can be computed using the k- ϵ model.

A clear drawback of this simple, but popular, model is that many other mechanisms of momentum interchange are not taken into account. For example, the so-called virtual mass force, the lateral lift force, the interfacial pressure distributions and the turbulent dispersion terms are all missing. Indeed, it is now well known that it is necessary to use a model that takes into account these mechanisms.

A more complete two-fluid model can be derived using "cell model" ensemble average techniques. This model is rigorous for a dilute dispersion of spherical bubbles in an inviscid flow with weak void and velocity gradients. The resulting phasic momentum equations are:

$$\begin{aligned} \frac{\partial}{\partial t} (\alpha_g \rho_g \underline{v}_g) + \nabla \cdot (\alpha_g \rho_g \underline{v}_g \underline{v}_g) = \nabla \cdot [\alpha_g \underline{\sigma}_s] + \nabla \cdot [\alpha_g (\underline{\tau}_g + \underline{\tau}_g^{Re})] \\ - \alpha_g \nabla p_\ell - C_{vm} \alpha_g \rho_\ell \underline{a}_{vm} - C_{rot} \alpha_g \rho_\ell \underline{v}_r \times \nabla \times \underline{v}_g \end{aligned}$$

$$\begin{aligned}
& - C_{vm}^* \rho_\ell \mathbf{y}_r \left(\frac{D_g \alpha_g}{Dt} + \alpha_g \nabla \cdot \mathbf{y}_g \right) - (C_1 - 2C_p) \alpha_g \rho_\ell \mathbf{y}_r \cdot \nabla \mathbf{y}_r^T \\
& - C_2 \alpha_g \rho_\ell \mathbf{y}_r \cdot \left[\nabla \mathbf{y}_r + \nabla \mathbf{y}_r^T + (\nabla \cdot \mathbf{y}_r) \underline{\underline{I}} \right] - b_s \rho_\ell (\mathbf{y}_r \cdot \mathbf{y}_r) \nabla \alpha_g \\
& - a_s \rho_\ell (\mathbf{y}_r \cdot \nabla \alpha_g) \mathbf{y}_r - C_L \rho_\ell \alpha_g \mathbf{y}_r \times \nabla \times \mathbf{y}_\ell + \alpha_g \rho_g \underline{\underline{g}} - \frac{C_D}{8} \rho_\ell A_i''' \mathbf{y}_r |\mathbf{y}_r| \quad (6a)
\end{aligned}$$

$$\begin{aligned}
& \frac{\partial}{\partial t} (\alpha_\ell \rho_\ell \mathbf{y}_\ell) + \nabla \cdot (\alpha_\ell \rho_\ell \mathbf{y}_\ell \mathbf{y}_\ell) = \nabla \cdot \left[\alpha_\ell \left(\underline{\underline{\tau}}_{\ell(BI)}^{Re} + \underline{\underline{\tau}}_{\ell(SI)}^{Re} \right) \right] \\
& - \alpha_\ell \nabla p_\ell - C_p \rho_\ell |\mathbf{y}_r|^2 \nabla \alpha_\ell + C_{vm} \alpha_g \rho_\ell \mathbf{a}_{vm} + C_{rot} \alpha_g \rho_\ell \mathbf{y}_r \times \nabla \times \mathbf{y}_g \\
& + C_{vm}^* \rho_\ell \mathbf{y}_r \left(\frac{D_g \alpha_g}{Dt} + \alpha_g \nabla \cdot \mathbf{y}_g \right) + C_1 \alpha_g \rho_\ell \mathbf{y}_r \cdot \nabla \mathbf{y}_r^T \\
& + C_2 \alpha_g \rho_\ell \mathbf{y}_r \cdot \left[\nabla \mathbf{y}_r + \nabla \mathbf{y}_r^T + (\nabla \cdot \mathbf{y}_r) \underline{\underline{I}} \right] \\
& + b_s \rho_\ell (\mathbf{y}_r \cdot \mathbf{y}_r) \nabla \alpha_g + a_s \rho_\ell (\mathbf{y}_r \cdot \nabla \alpha_g) \mathbf{y}_r + C_L \rho_\ell \alpha_g \mathbf{y}_r \times \nabla \times \mathbf{y}_\ell \\
& + \alpha_\ell \rho_\ell \underline{\underline{g}} + \frac{C_D}{8} \rho_\ell A_i''' \mathbf{y}_r |\mathbf{y}_r| \quad (6b)
\end{aligned}$$

where, the virtual mass acceleration is,

$$\mathbf{a}_{vm} = \left(\frac{\partial}{\partial t} + \mathbf{y}_g \cdot \nabla \right) \mathbf{y}_g - \left(\frac{\partial}{\partial t} + \mathbf{y}_\ell \cdot \nabla \right) \mathbf{y}_\ell = \frac{D_g \mathbf{y}_g}{Dt} - \frac{D_\ell \mathbf{y}_\ell}{Dt}$$

and, for spherical noninteracting bubbles:

$$\begin{aligned}
a_\ell &= -\frac{1}{20}, & a_s &= -\frac{9}{20}, & \hat{a}_s &= -\frac{9}{20}, \\
b_\ell &= -\frac{3}{20}, & b_s &= \frac{3}{20}, & \hat{b}_s &= \frac{3}{20}.
\end{aligned}$$

In order to numerically evaluate this two-fluid model we need the appropriate boundary conditions. There is no general theory for the type of boundary and initial conditions that a system of partial differential equations requires in order

to have a unique solution. Nevertheless, for a hyperbolic system Cauchy conditions are recommended.

Most researchers in the past have evaluated two-phase models as initial value problems using parabolic numerical techniques, thus it was not necessary to specify boundary conditions at the outlet of the integration domain. However, when this approach is used, one has to specify the pressure distribution in the integration domain. For many cases a hydrostatic pressure distribution is a good approximation. Unfortunately, when a parabolic scheme is used, one cannot compute flow recirculation. In particular, one cannot compute gas flow reversal, an important feature in the two-phase jets which are of interest in this study.

In this work we have used an elliptic (ie, boundary value) calculational scheme. That is, we have numerically evaluated the full two-fluid model and the associated k-ε model using appropriate boundary conditions at the inlet and the exit. This complicates the evaluation procedure, however only in this way can we obtain a prediction of gas flow reversal.

Figure-1 shows the integration domain. We have refined the grid near the symmetry plane of the planar jet because the gradients are the steepest there. In the axial (i.e., z) direction we have increasingly larger cells because of the decreasing gradients. The boundary conditions which have been used are:

INLET ($z = 0, -\frac{h}{2} \leq y \leq \frac{h}{2}$)

$$\text{Gas mass flux} = \alpha \rho_g V \quad (7a)$$

$$\text{Liquid mass flux} = (1 - \alpha) \rho_l V \quad (7b)$$

$$u_{ty} = 0 \quad (7c)$$

$$u_{gy} = 0 \quad (7d)$$

$$u_{tz} = V \quad (7e)$$

$$u_{gz} = V \quad (7f)$$

$$\text{Kinetic energy} \equiv k = \frac{3}{2} (u'_{tz})^2 \quad (7g)$$

$$\text{Dissipation} \equiv \epsilon = \frac{0.1643 (u'_{tz})^3}{(0.09 h)} = 1.8256 (u'_{tz})^3 / h \quad (7h)$$

OUTLET ($z = Z$)

$$p = \rho_l g \cos \theta Z \quad (8a)$$

$$\frac{\partial u_{ly}}{\partial z} = 0 \quad \frac{\partial u_{gy}}{\partial z} = 0 \quad (8b)$$

$$\frac{\partial u_{lz}}{\partial z} = 0 \quad \frac{\partial u_{gz}}{\partial z} = 0 \quad (8c)$$

$$\frac{\partial k}{\partial t} = 0 \quad \frac{\partial \epsilon}{\partial z} = 0 \quad (8d)$$

It should be noted that the boundary conditions associated with the mass balances are only required at the inlet. This can be understood based on the fact that the mass balance is a first order partial differential equation. Moreover, given the velocity field, the equation may be solved for the void fraction along the model's characteristics. With the void fraction given at the inlet, the void fraction field can be readily evaluated.

Because the velocity fields, as well as the turbulent kinetic energy and the dissipation, are not well known at the outlet, we have specified natural boundary conditions. That is, we set the gradients of these variables in the flow direction equal to zero. In our case the outlet boundary conditions were found to have a negligible effect except for the last two rows of cells.

The numerical results presented herein correspond to a planar liquid jet impacting a liquid pool using the two-fluid model given by Eqs. (1) and (5). The liquid jet velocity at the location of impact was $u_{lz} = 5$ m/s, and a constant bubble diameter of 2 mm was assumed. The initial velocity profile was uniform. The jet width, h , was 4.03 mm, and the void fraction at the location of impact was assumed to be uniform and equal to 5%. The inlet turbulent intensity was 3% and the inlet turbulent dissipation was computed using Eq. (7h). The inclination angle of the jet was measured with respect to the vertical plane (i.e. $\theta = 0$ degrees means a vertical planar jet). The integration domain had an extent of $y = 0.2$ m in the lateral direction and $z = 0.25$ m in the axial direction. The k - ϵ model for turbulence used the constant values suggested by Launder & Spalding for single-phase flow. We have presented results corresponding to a vertical liquid jet ($\theta = 0$ degrees) unless otherwise stated.

Figure-2 shows the gas and liquid axial velocities as a function of lateral direction for $z = 0.225$ m (note, $y = 0.1$ m is the jet's plane of symmetry). Both velocity profiles show a Gaussian-like profile. We see that, due to buoyancy, the liquid velocity is always higher than the gas velocity, a well-known characteristic of

downflows. The relative velocity was approximately 0.3 m/s which is very close to the terminal rise velocity of the bubbles.

Figure-3 depicts the axial liquid velocity as a function of lateral position for different axial positions. The curve labeled, $z = 0.00125$ m, is right under the impacting location and one can see an almost uniform velocity profile ($u_z \approx 5$ m/s). As we move down in the pool the jet is dispersed due to momentum interchange with the surrounding fluid. The curve $z = 0.225$ m is the same one shown in Figure 2.

Figure-4 shows the turbulent kinetic energy, k , as a function of lateral position for $z = 0.225$ m. The curve shows the characteristic relative minimum in k at the symmetry plane.

In Figure-5 the liquid velocity field has been plotted as a function of axial and lateral position. The length of the arrows is proportional to the liquid velocity at the location of the arrow's tail. The arrow's tail is located at the center of the computational cell. The arrow scale is in the lower left corner ($u_{z\ell} = 2$ m/s). The spreading of the jet can be easily seen in this plot as noted previously. Near the location of jet impact ($z = 0$) the axial velocity is almost uniform. Because of the momentum interchange between the jet and the surrounding fluid, liquid is entrained in the lateral, y , direction. Finally, one may note the formation of two weak recirculation zones near the y -boundaries for large z .

Figure-6 shows a contour plot of the axial liquid velocity. The lines connect positions with the same axial velocity (equivelocity lines). The outer curve corresponds to $u_{z\ell} = 0.25$ m/s, and the difference between successive lines is 0.25 m/s.

Figure-7 shows a contour plot of the void fraction for one half of the jet. The outer line connects points with the void fraction $\alpha = 0.25\%$. The divergent lines show that, when only drag is used for closure, the void fraction field spreads only slightly as z increases.

Figure-8 shows a vector plot of the liquid velocity field for an inclined planar jet ($\theta = 45^\circ$). We rotate the integration domain 45° in order to have the plane $y = 0$ aligned with the jet orientation. This was done for computer time economy purposes and in order to minimize numerical diffusion. It can be seen that, as expected, the gas drags the liquid away from the centerplane.

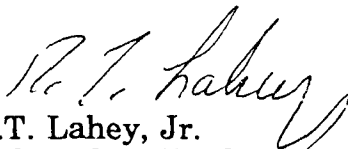
Figure-9 shows a vector plot of the gas velocity field for an inclined planar jet ($\theta = 45^\circ$). Of particular interest are the results shown in the upper right corner, the gas velocity (weighted with the void fraction) at the y -boundary. This shows a reversal of the gas flow rate.

Dr. Edwin R. Rood
October 22, 1992
Page 8

The calculations presented herein correspond to a simple two-fluid model. The calculations corresponding to the full two-fluid model (ie, using Eqs. (7)) are currently under way. These predictions, and the plunging liquid jet data using a planar nozzle, are expected to be available during the next report period.

If you have any questions concerning this report, please contact me or Professor Drew at your convenience [Lahey: (518) 276-8579; Drew: (518) 276-6903].

Sincerely yours,



Dr. R.T. Lahey, Jr.
The Edward E. Hood, Jr. Professor of Engineering

RTL/ev

cc: Administrative Grants Officer
Director, Naval Research Laboratory
Defense Technical Information Center ✓
D.A. Drew (RPI)
F. Bonetto (RPI)

Fig. 1 Discretization of the Integration Domain

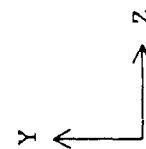
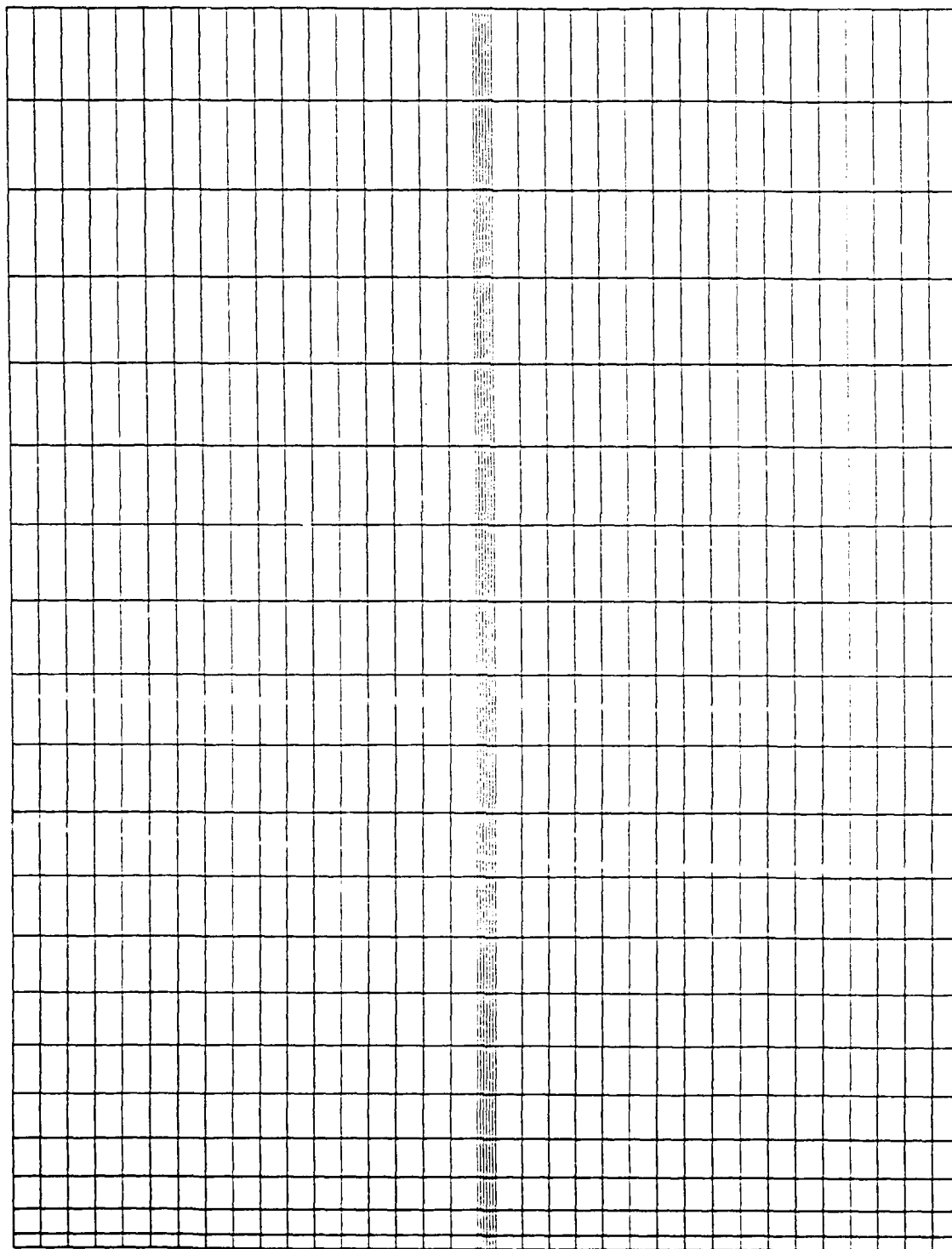


Fig. 2 Liquid and Gas Velocity Profiles for an Axial Position
 $z = 0.225$ m

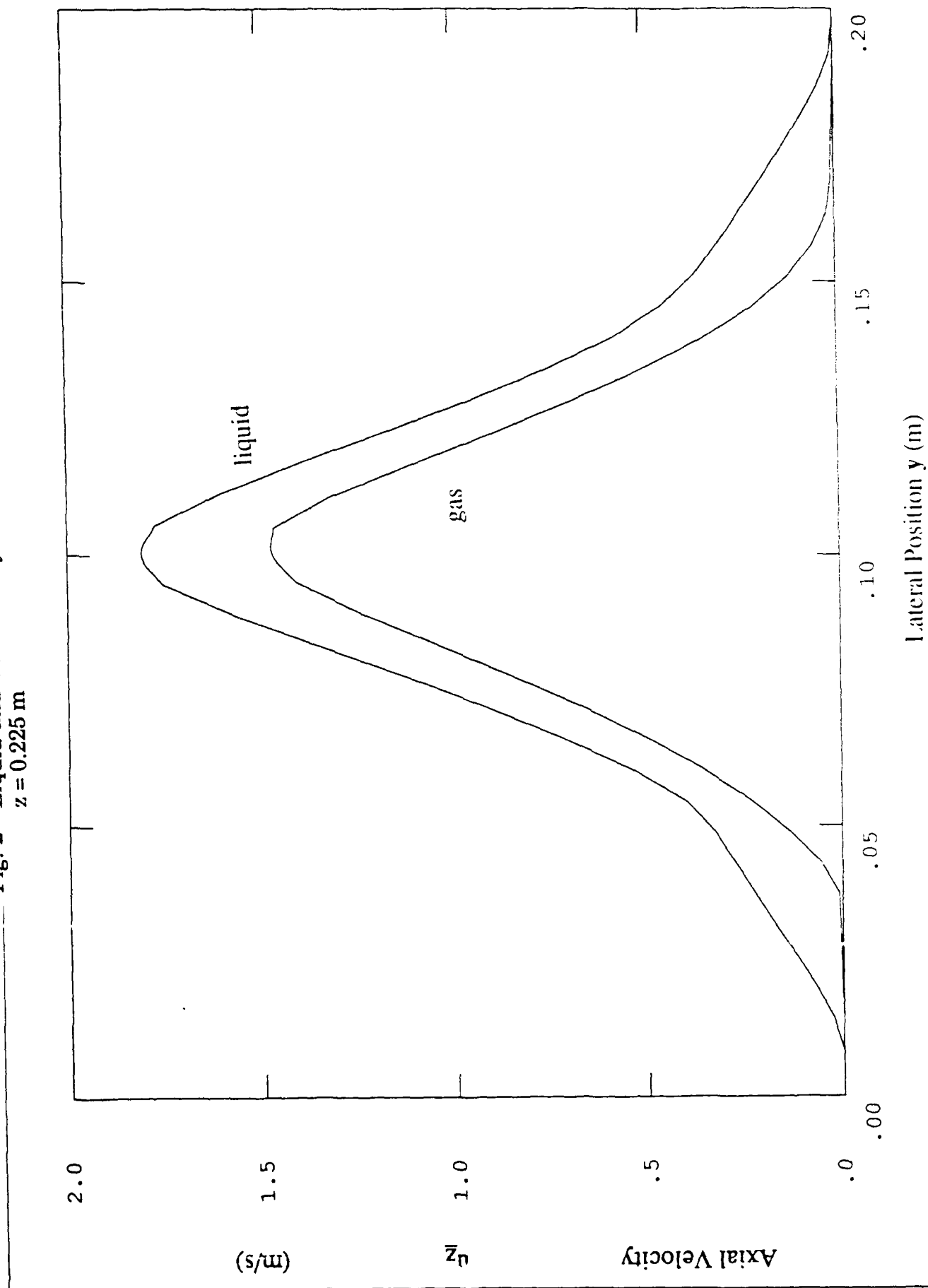


Fig. 3 Liquid Velocity Profiles for Four Different Axial Positions

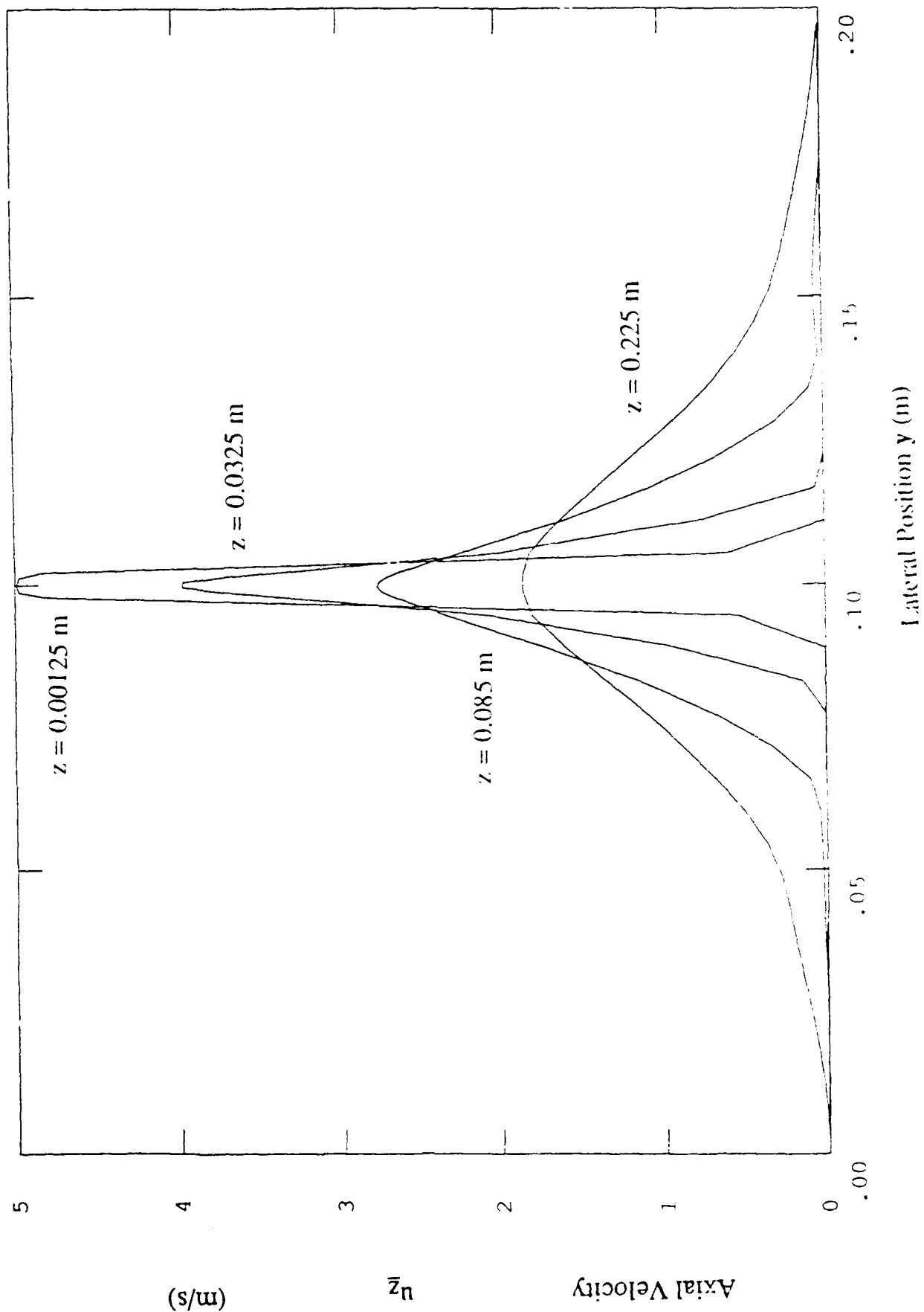


Fig. 4 Turbulent Kinetic Energy Profiles for $z = 0.225$ m

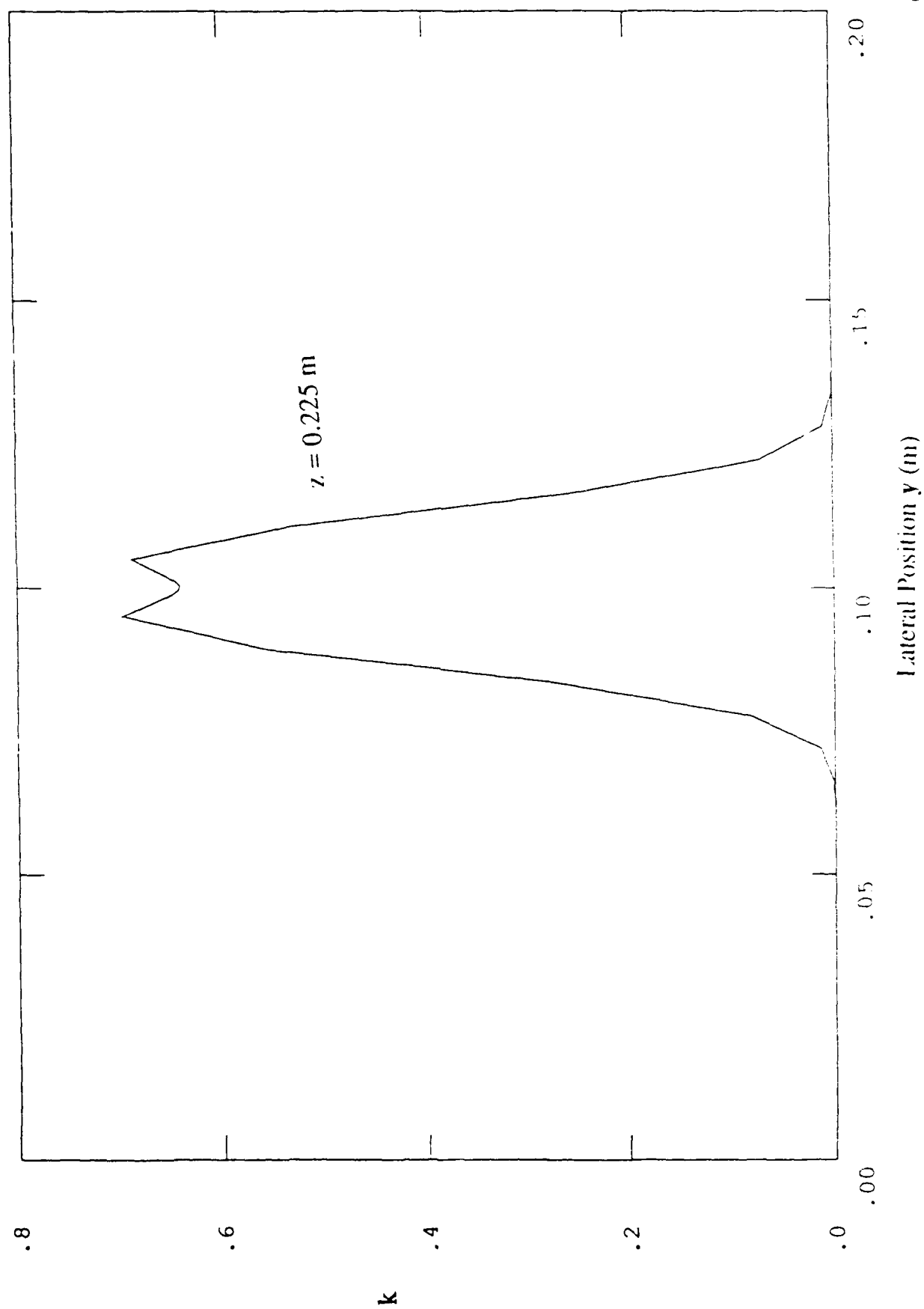
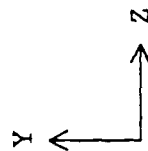
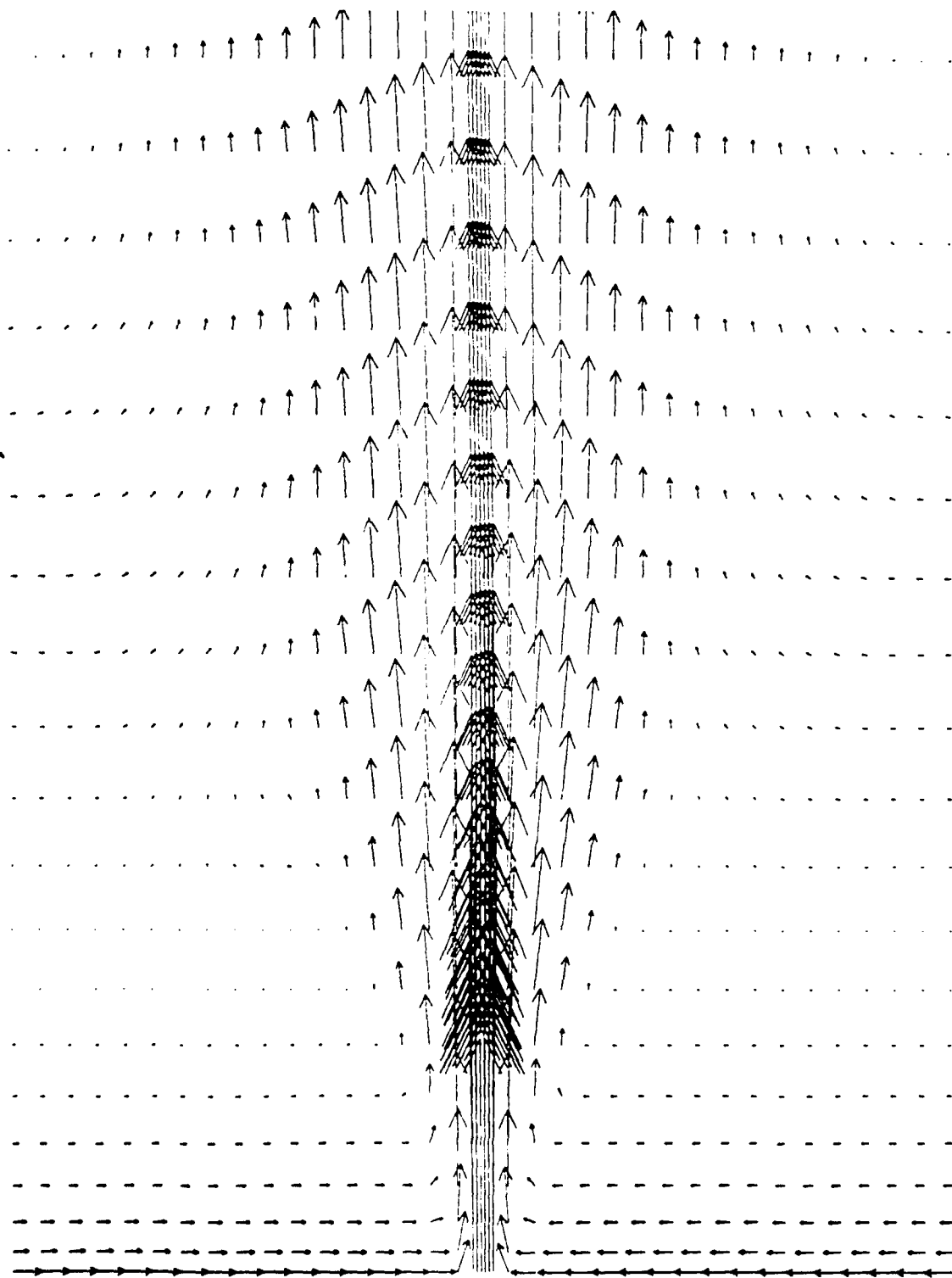


Fig. 5 Vector Plot of the Liquid Velocity for $\theta = 0^\circ$

$\theta = 0$ degrees

liquid



→ : 2.00 m/s.

K-EP, PLANAR JET, ELLIPTIC, FABIAN, 1 PHASE,

PHOENICS

Fig. 6 Contour Plot of the Axial Liquid Velocity for $\theta = 0^\circ$

$\theta = 0$ degrees
liquid

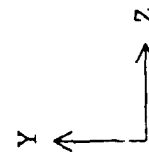
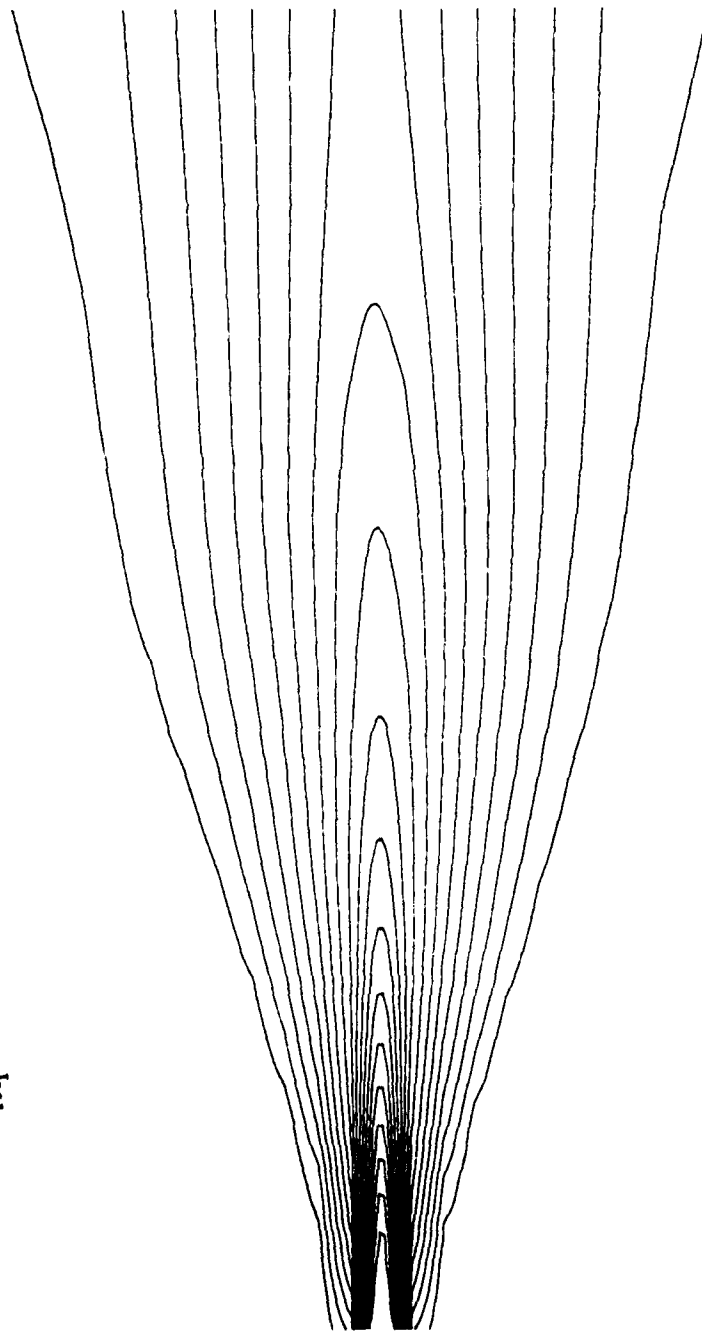


Fig. 7 Contour Plot of the Void Fraction (Half of the Jet) for the Vertical Jet
($\theta = 0^\circ$)

$\theta = 0$ degrees
gas

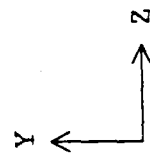
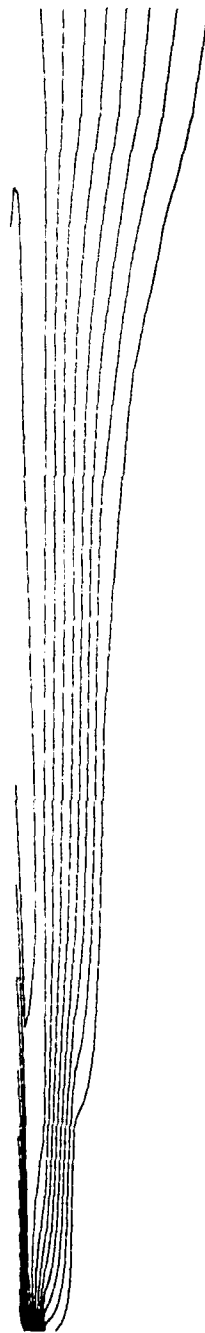
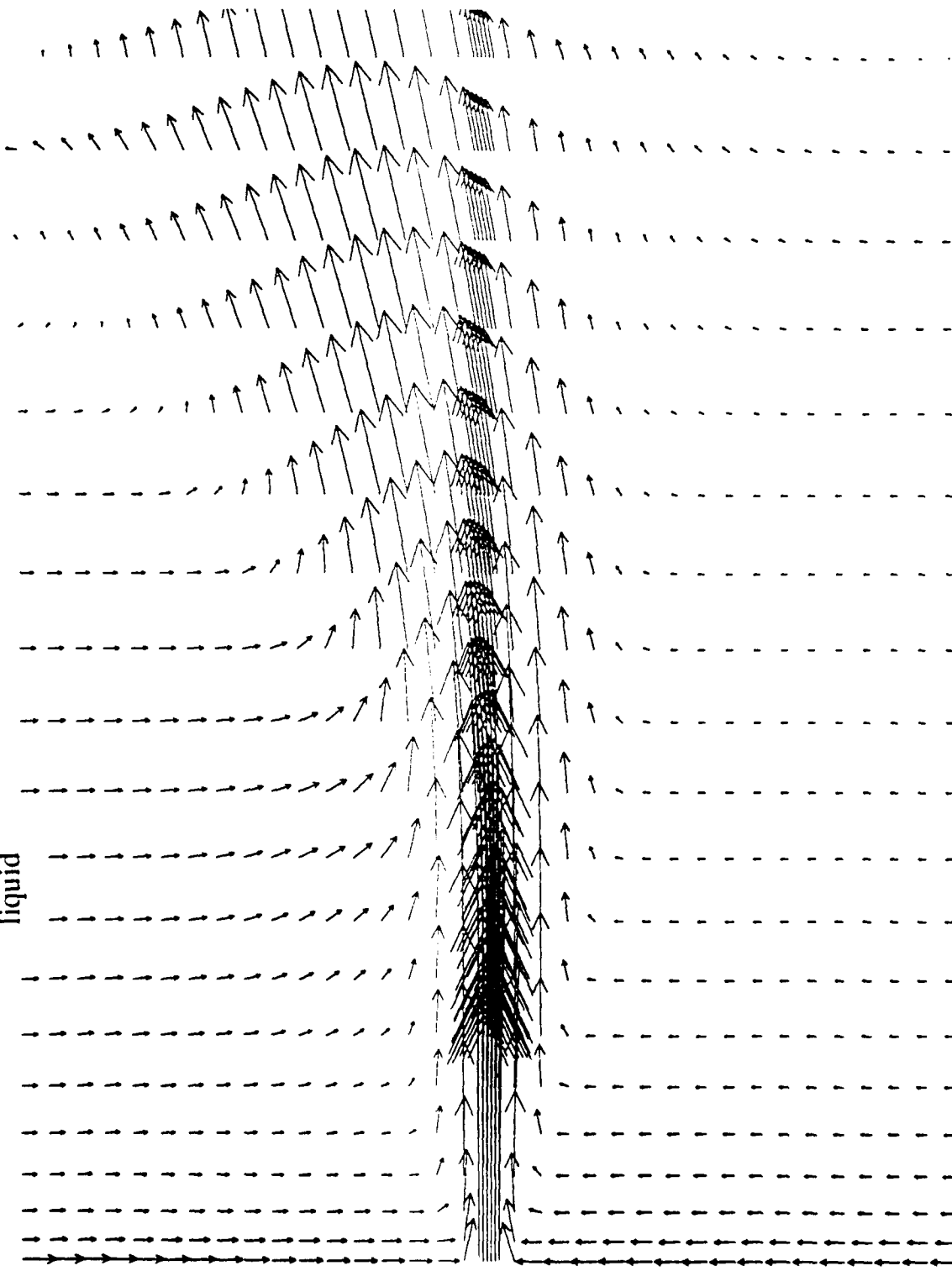


Fig. 8 Vector Plot of the Liquid Velocity for the Inclined Jet ($\theta = 45^\circ$)

$\theta = 45$ degrees

liquid



→ : 2.00 m/s.



$\bar{u}_l(45^\circ)$

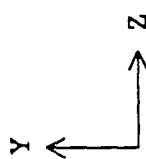
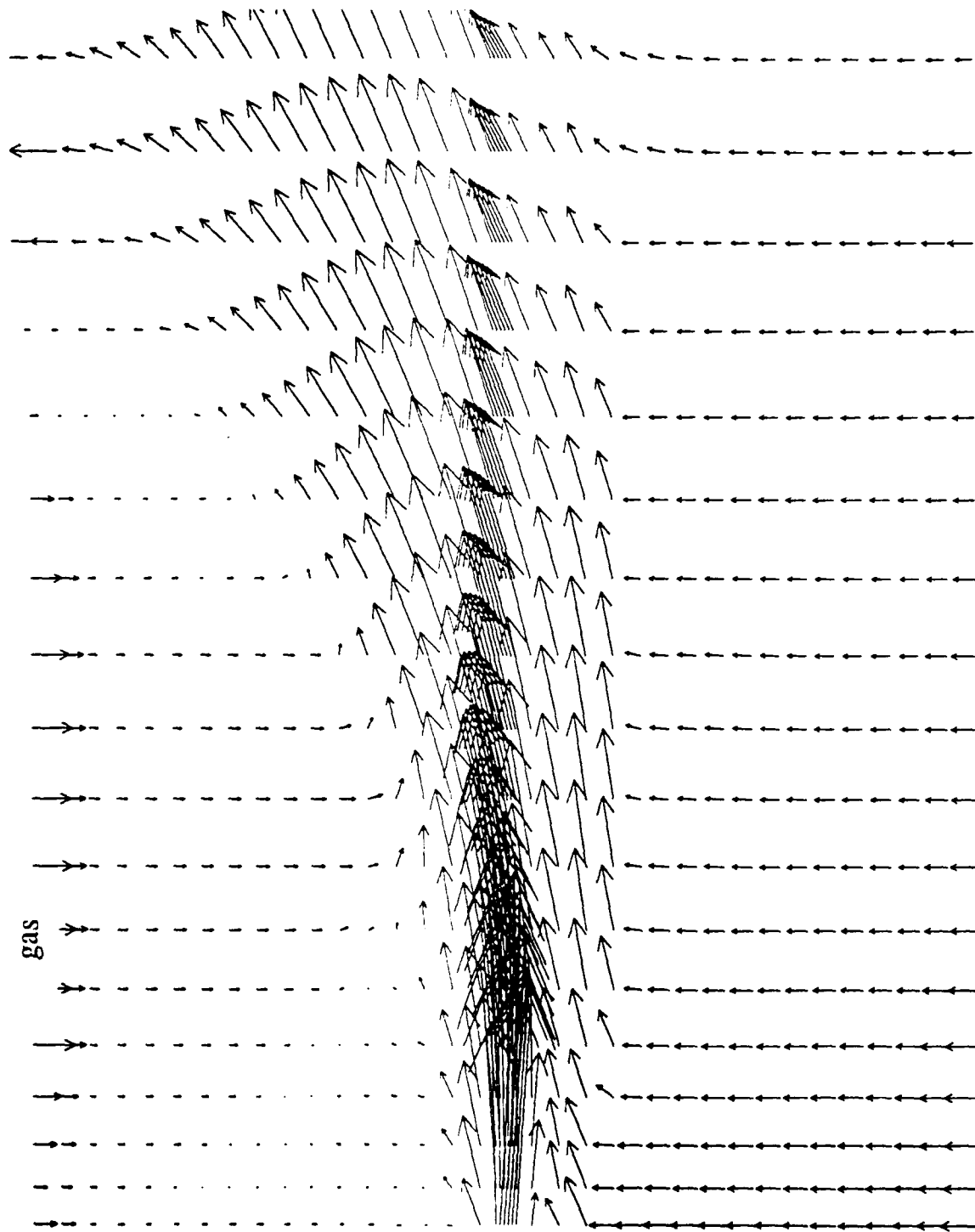


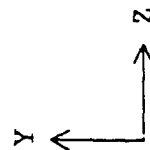
Fig. 9 Vector Plot of the Gas Velocity for the Inclined Jet ($\theta = 45^\circ$)

$\theta = 45$ degrees

gas



$\bar{u}_g(45^\circ)$



→ : 2.00 m/s.

K-EP, PLANAR JET, ELLIPTIC, FABIAN, I PHASE,

PHOENICS